On Mechanical Modeling of Cantilevered Piezoelectric Vibration Energy Harvesters

A. ERTURK[1,*] AND D. J. INMAN[2]

[1]*Department of Engineering Science and Mechanics*

[2]*Department of Mechanical Engineering, Center for Intelligent Material Systems and Structures, Virginia Tech Blacksburg, VA 24061, USA*

ABSTRACT: Cantilevered beams with piezoceramic (PZT) layers are the most commonly investigated type of vibration energy harvesters. A frequently used modeling approach is the single-degree-of-freedom (SDOF) modeling of the harvester beam as it allows simple expressions for the electrical outputs. In the literature, since the base excitation on the harvester beam is assumed to be harmonic, the well known SDOF relation is employed for mathematical modeling. In this study, it is shown that the commonly accepted SDOF harmonic base excitation relation may yield highly inaccurate results for predicting the motion of cantilevered beams and bars. First, the response of a cantilevered Euler–Bernoulli beam to general base excitation given in terms of translation and small rotation is reviewed where more sophisticated damping models are considered. Then, the error in the SDOF model is shown and correction factors are derived for improving the SDOF harmonic base excitation model both for transverse and longitudinal vibrations. The formal way of treating the components of mechanical damping is also discussed. After deriving simple expressions for the electrical outputs of the PZT in open-circuit conditions, relevance of the electrical outputs to vibration mode shapes and the electrode locations is investigated and the issue of strain nodes is addressed.

Key Words: energy harvesting, mechanical modeling, base excitation, damping, strain nodes.

INTRODUCTION

THE idea of harvesting ambient vibration energy to power small electronic components has been discussed by several authors in the last five years (Sodano et al., 2004; Beeby et al., 2006). Among the different approaches for converting the mechanical vibration energy to electric energy, the most popular harvester mechanism used is a cantilevered beam with piezoceramic (PZT) layers. Typically, the cantilevered beam is attached to a vibrating/moving host structure and therefore it is subjected to a base excitation. For the sake of simplicity, most of the authors have considered the base excitation to be harmonic in time. Furthermore, in order to obtain closed-form electromechanical expressions for the resulting voltage and power outputs and also to optimize the system parameters in a simple manner, several authors have used single-degree-of-freedom (SDOF) modeling. Since the base excitation is assumed to be harmonic, the well-known SDOF harmonic base excitation relation (which is available in any elementary vibration textbook) has been widely used for modeling the dynamics of the problem.

The early discussion of Williams and Yates (1996) on the generated power was based on the SDOF harmonic base excitation relation. Although they focused on electromagnetic type of vibration energy harvesters, El-Hami et al. (2001) also built their formulation on the same mechanical SDOF relation. A 1-D electromechanically coupled piezoelectric generator model was presented by duToit et al. (2005) where they introduced the electrical effects to the SDOF harmonic base excitation relation. Stephen (2006) discussed the maximum power generation and the effect of mechanical damping using the same SDOF relation. Quite recently, Ajitsaria et al. (2007) employed the SDOF relation for predicting the voltage output analytically. Some authors (Jeon et al., 2005; Fang et al., 2006) employed the SDOF base excitation relation just to represent the mathematical problem although they did not provide detailed formulation. In short, the SDOF modeling and/or representation of the base excitation relation are widely used in vibration energy harvesting literature, which provides sufficient motivation to compare its accuracy against the distributed parameter solution that uses the Euler–Bernoulli beam model. Furthermore, reviewing the formal solution

*Author to whom correspondence should be addressed.
E-mail: erturk@vt.edu
Figures 3–7, 9, 11 and 12 appear in color online: http://jim.sagepub.com

1045-389X/08/11 1311–15 $10.00/0 DOI: 10.1177/1045389X07085639

procedure of the base excitation problem for a cantilevered Euler–Bernoulli beam might be appropriate considering the incorrect approaches to the same problem due to weak mathematical assumptions. For instance, recently, Ajitsaria et al. (2007) attempted to represent the base excitation (which is, indeed, a distributed force on the beam) as a tip force to obtain a SDOF representation. Other flaws in the same work, such as the fact that Ajitsaria et al. (2007) combined the static piezoelectric actuation equations taken from the literature with the dynamic Euler–Bernoulli beam equation, are beyond the discussion of this study which intends to examine mainly the mechanical side of the problem.

In this study, first the general solution of the base excitation problem for transverse vibrations of a cantilevered Euler–Bernoulli beam is reviewed and the formal treatment of mechanical damping is discussed. The aspect ratios of typical harvester beams used in the literature allow neglecting the effects of shear deformation and rotary inertia, and make it reasonable to use the Euler–Bernoulli beam model. The base motion is described by translation and small rotation and it is not restricted to be harmonic in time. Then the general solution is reduced to the particular case of harmonic base translation and the results of the Euler–Bernoulli model are compared with those of the SDOF model in a nondimensional basis. It is shown that the SDOF model may yield highly inaccurate results and a correction factor is derived for improving the SDOF model for transverse vibrations. The variation of correction factor with tip mass to beam mass ratio is also given and it is observed that the uncorrected SDOF model can be accurate only when this ratio is sufficiently high. The base excitation problem is summarized for the case of longitudinal vibrations and a correction factor is introduced also for the SDOF harmonic base excitation model of longitudinal vibrations. After summarizing the relevance of the correction factor to the SDOF electromechanical equations, simple expressions are derived for the electrical outputs of PZT in open-circuit conditions. These expressions lead to important conclusions regarding the effect of strain nodes of the beam on the electrical outputs which can be important especially if the harvester is not excited at its fundamental natural frequency. The concept of the effects of strain mode shapes on the harvested energy was eluded to in duToit et al. (2005), and it is precisely examined and clarified here.

BASE EXCITATION PROBLEM FOR TRANSVERSE VIBRATIONS OF A CANTILEVERED BEAM

Response to General Base Excitation

The uniform clamped-free Euler–Bernoulli beam shown in Figure 1 is subjected to the arbitrary translation $g(t)$ and small rotation $h(t)$ of its base. For the purpose of demonstration, this harvester beam (or the bender) is shown as a unimorph bender having two layers: the substructure layer (at the bottom) and the PZT layer (at the top). However, it could as well be a bimorph configuration with two PZT layers bracketing the substructure layer. In practice, the PZT layer is connected to a harvesting circuit through the conductive electrodes (which can be combined in series or in parallel depending on the voltage or current requirements if the configuration is a bimorph). Examination of the electric circuit models and the various piezoelectric harvester configurations is not the focus of this study, which aims to discuss some important mechanical aspects. From the mechanical point of view, the configuration of the layers is expected to affect the flexural stiffness and the mass per unit length of the beam, which can be handled by using the following approach as long as the beam is uniform along its longitudinal axis. In order to discuss the mechanical aspects in a simple manner, the electromechanical effects in the mechanical domain due to the piezoelectric effect and a possible electric circuit are ignored. The coupled electromechanical behavior of the distributed parameter harvester beam and a simple electric circuit connected to it has been investigated by the authors recently (Erturk and Inman, 2008).

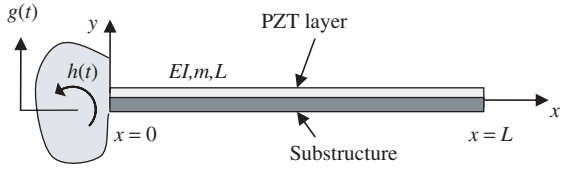

Figure 1. *Cantilevered bender under translational and small rotational base motions.*

The absolute displacement of the beam at any point x along the beam axis in the transverse direction (i.e., in y-direction) is denoted by $w(x, t)$. If the beam is assumed to be undamped, the equation of motion for free vibrations in the absolute x–y frame can be written as (Timoshenko et al., 1974):

$$EI\frac{\partial^4 w(x,t)}{\partial x^4} + m\frac{\partial^2 w(x,t)}{\partial t^2} = 0 \tag{1}$$

where EI is the flexural stiffness (E is the Young's modulus and I is the cross-sectional area moment of inertia) and m is the mass per unit length of the beam. Note that the way of obtaining the equivalent flexural stiffness of a beam with composite cross-section is described in elementary strength of materials books (e.g., Beer and Johnston, 1992). For the sake of completeness, the tip mass (or the so-called proof mass) is excluded and the effect of a tip mass on the formulation can be found in a recent study by

Erturk and Inman (2007) and its effects on the results will be summarized later in this study.

Two types of damping mechanisms will be included to the undamped beam: viscous air (medium) damping and Kelvin–Voigt (or strain-rate) damping. Hence the equation of motion of the damped beam becomes

$$EI\frac{\partial^4 w(x,t)}{\partial x^4}+c_s I\frac{\partial^5 w(x,t)}{\partial x^4\partial t}+c_a\frac{\partial w(x,t)}{\partial t}+m\frac{\partial^2 w(x,t)}{\partial t^2}=0 \tag{2}$$

where c_a is the viscous air damping coefficient and c_s is the strain-rate damping coefficient. Viscous air damping is a simple way of modeling the force acting on the beam due to the air particles displaced by the beam during the vibratory motion and strain-rate damping accounts for the structural damping due to the friction internal to the beam (Banks and Inman, 1991). Both of these damping mechanisms satisfy the proportional damping criteria and hence they are mathematically convenient for the modal analysis solution procedure. Other beam damping mechanisms and the identification procedures of their respective damping parameters from experimental measurements were discussed by Banks and Inman (1991).

As suggested by Timoshenko et al. (1974), the absolute transverse motion of the beam at any point x and time t can be written as:

$$w(x,t)=w_b(x,t)+w_{rel}(x,t) \tag{3}$$

where $w_{rel}(x,\ t)$ is the transverse displacement relative to the clamped end of the beam and $w_b(x,\ t)$ is the base motion given by

$$w_b(x,t)=\delta_1(x)g(t)+\delta_2(x)h(t). \tag{4}$$

Here, $\delta_1(x)$ and $\delta_2(x)$ are the displacement influence functions for the transverse base displacement and small base rotation of the beam, respectively. For the cantilevered beam case, $\delta_1(x)=1$ and $\delta_2(x)=x$ (Timoshenko et al., 1974). Using Equation (3) in Equation (2) yields

$$EI\frac{\partial^4 w_{rel}(x,t)}{\partial x^4}+c_s I\frac{\partial^5 w_{rel}(x,t)}{\partial x^4\partial t}+c_a\frac{\partial w_{rel}(x,t)}{\partial t}+m\frac{\partial^2 w_{rel}(x,t)}{\partial t^2}=-m\frac{\partial^2 w_b(x,t)}{\partial t^2}-c_a\frac{\partial w_b(x,t)}{\partial t}. \tag{5}$$

Note that, after expressing the absolute transverse motion $w(x,\ t)$ in terms of the base motion $w_b(x,\ t)$ and relative transverse motion $w_{rel}(x,\ t)$, the free vibration equation for the absolute motion of the beam given by Equation (2) becomes a forced vibration equation for the relative vibratory motion of the beam. There are two important points to mention at this stage. First, air damping acts on the absolute velocity whereas the strain-rate damping acts on the relative velocity of the beam. As a consequence, the attempts (duToit et al., 2005) for including 'all sources of mechanical damping' in a single damping coefficient are oversimplified. Second, for the same reason, the excitation is not only due to the rigid body inertia of the beam but also due to the effect of air damping on the rigid body motion. The latter may or may not be negligible depending on the nature of external damping, which will be discussed later in this study.

The boundary conditions for the relative vibratory motion of the beam can be written as:

$$w_{rel}(0,t)=0,\left.\frac{\partial w_{rel}(x,t)}{\partial x}\right|_{x=0}=0, \tag{6}$$

$$\left[EI\frac{\partial^2 w_{rel}(x,t)}{\partial x^2}+c_s I\frac{\partial^3 w_{rel}(x,t)}{\partial x^2\partial t}\right]_{x=L}=0,$$

$$\left[EI\frac{\partial^3 w_{rel}(x,t)}{\partial x^3}+c_s I\frac{\partial^4 w_{rel}(x,t)}{\partial x^4\partial t}\right]_{x=L}=0. \tag{7}$$

Note that the strain-rate damping results in a moment as well as a transverse force term that appears in the natural boundary conditions written for the free end (Banks and Inman, 1991). Following the standard modal expansion method, the solution of Equation (5) can be represented by an absolutely and uniformly convergent series of the eigenfunctions as:

$$w_{rel}(x,t)=\sum_{r=1}^{\infty}\phi_r(x)\eta_r(t) \tag{8}$$

where $\phi_r(x)$ and $\eta_r(t)$ are the mass normalized eigenfunction and the modal coordinate of the clamped-free beam for the rth mode, respectively. Since the system is proportionally damped, the eigenfunctions denoted by $\phi_r(x)$ are indeed the mass normalized eigenfunctions of the corresponding undamped free vibration problem (Caughey and O'Kelly, 1965) given by Equation (1) along with the clamped-free boundary conditions

$$w_{rel}(0,t)=0,\left.\frac{\partial w_{rel}(x,t)}{\partial x}\right|_{x=0}=0,$$

$$EI\left.\frac{\partial^2 w_{rel}(x,t)}{\partial x^2}\right|_{x=L}=0,\quad EI\left.\frac{\partial^3 w_{rel}(x,t)}{\partial x^3}\right|_{x=L}=0. \tag{9}$$

Therefore, the resulting mass normalized eigenfunction of the rth mode is

$$\phi_r(x)=\sqrt{\frac{1}{mL}}\left[\cosh\frac{\lambda_r}{L}x-\cos\frac{\lambda_r}{L}x-\sigma_r\left(\sinh\frac{\lambda_r}{L}x-\sin\frac{\lambda_r}{L}x\right)\right] \tag{10}$$

where the λ_rs are the dimensionless frequency numbers obtained from the characteristic equation given by:

$$1 + \cos\lambda \cosh\lambda = 0 \tag{11}$$

and σ_r is expressed as:

$$\sigma_r = \frac{\sinh\lambda_r - \sin\lambda_r}{\cosh\lambda_r + \cos\lambda_r}. \tag{12}$$

It should be noted that Equations (10)–(12) are valid for a clamped-free beam without a tip mass. The eigenfunction and the characteristic equation expressions for a clamped-free beam with a tip mass can be found in a recent work by Erturk and Inman (2007). The presence of a tip mass also affects the right-hand side of a Equation (5) since the rigid body inertia of the tip mass also contributes to the excitation of the beam in that case.

The mass normalized form of the eigenfunctions given by Equation (10) satisfies the orthogonality conditions:

$$\int_{x=0}^{L} m\phi_s(x)\phi_r(x)dx = \delta_{rs}, \quad \int_{x=0}^{L} EI\phi_s(x)\frac{d^4\phi_r(x)}{dx^4}dx = \omega_r^2\delta_{rs} \tag{13}$$

where δ_{rs} is the Kronecker delta, defined as being equal to unity for $s = r$ and equal to zero for $s \neq r$, and ω_r is the undamped natural frequency of the rth mode given by:

$$\omega_r = \lambda_r^2\sqrt{\frac{EI}{mL^4}}. \tag{14}$$

The modal response is the solution of the following ordinary differential equation

$$\frac{d^2\eta_r(t)}{dt^2} + 2\zeta_r\omega_r\frac{d\eta_r(t)}{dt} + \omega_r^2\eta_r(t) = N_r(t). \tag{15}$$

where

$$2\zeta_r\omega_r = \frac{c_s\omega_r^2}{E} + \frac{c_a}{m}. \tag{16}$$

Therefore, the damping ratio ζ_r includes the effects of both strain-rate damping and viscous air damping and it can be expressed as $\zeta_r = \zeta_r^s + \zeta_r^a$ where the strain-rate and the air damping components of the damping ratio are $\zeta_r^s = c_s\omega_r/2E$ and $\zeta_r^a = c_a/2m\omega_r$, respectively. It is clear from Equation (16) that the strain-rate damping coefficient is proportional to structural stiffness and the viscous air damping coefficient is proportional to mass per unit length. This type of damping is also known as the Rayleigh damping (Clough and Penzien, 1975). It is worthwhile to mention that evaluation of the proportional damping coefficients c_s and c_a (from experimental measurements) requires knowing the natural frequencies and modal damping ratios of two separate modes (Clough and Penzien, 1975). If one knows the natural frequencies (ω_j, ω_k) and the modal damping ratios[1] (ζ_j, ζ_k) of modes j and k, it is straightforward from Equation (16) to obtain the c_s and c_a values using[2]

$$\begin{Bmatrix} c_s \\ c_a \end{Bmatrix} = \frac{2\omega_j\omega_k}{\omega_j^2 - \omega_k^2}\begin{bmatrix} \frac{E}{\omega_k} & -\frac{E}{\omega_j} \\ -m\omega_k & m\omega_j \end{bmatrix}\begin{Bmatrix} \zeta_j \\ \zeta_k \end{Bmatrix}. \tag{17}$$

In Equation (15), the modal forcing function $N_r(t)$ can be expressed as:

$$N_r(t) = N_r^m(t) + N_r^c(t). \tag{18}$$

Here, the inertial and the damping excitation terms are given by the following expressions, respectively:

$$\begin{aligned} N_r^m(t) &= -m\left(\gamma_r^w\frac{d^2g(t)}{dt^2} + \gamma_r^\theta\frac{d^2h(t)}{dt^2}\right) \\ N_r^c(t) &= -c_a\left(\gamma_r^w\frac{dg(t)}{dt} + \gamma_r^\theta\frac{dh(t)}{dt}\right) \end{aligned} \tag{19}$$

where

$$\gamma_r^w = \int_{x=0}^{L}\phi_r(x)dx, \quad \gamma_r^\theta = \int_{x=0}^{L}x\phi_r(x)dx. \tag{20}$$

Then, the modal response can be obtained by using the Duhamel integral as:

$$\eta_r(t) = \frac{1}{\omega_{rd}}\int_{\tau=0}^{t} N_r(\tau)e^{-\zeta_r\omega_r(t-\tau)}\sin\omega_{rd}(t-\tau)d\tau \tag{21}$$

where $\omega_{rd} = \omega_r\sqrt{1-\zeta_r^2}$ is the damped natural frequency of the rth mode. Eventually, the modal response obtained using Equation (21) can be used in Equation (8) along with the eigenfunction expression given by Equation (10) and the relative response $w_{rel}(x, t)$ at any point along the beam axis can be obtained as:

$$w_{rel}(x,t) = \sum_{r=1}^{\infty}\frac{\phi_r(x)}{\omega_{rd}}\int_{\tau=0}^{t} N_r(\tau)e^{-\zeta_r\omega_r(t-\tau)}\sin\omega_{rd}(t-\tau)d\tau. \tag{22}$$

Note that the displacement at the tip of the beam can be obtained by just setting $x = L$ in Equation (22). If one is interested, the absolute response of the beam can be obtained by just using the relative displacement and the

[1]One common way of obtaining the modal damping ratios is using the quality factor (Q) of the mode of interest (Inman, 2006).

[2]A more realistic approach for identifying these damping coefficients was described by Banks and Inman (1991).

base motion input in Equation (3). However, the main concern in vibration energy harvesting is the response of the beam relative to its base. The expression obtained for the relative motion of the beam, Equation (22), is not restricted to harmonic base excitation and it can handle transient base histories (including small base rotations).

Steady State Response to Harmonic Base Excitation

In most of the theoretical and experimental studies on piezoelectric energy harvesters, the base excitation is assumed to be harmonic translation for simplicity (although this is not the case for many ambient vibration sources). If the base translation is in the form of $g(t) = Y_0 e^{i\omega t}$ (where Y_0 is the excitation amplitude and ω is the excitation frequency) and if there is no rotational base excitation (i.e., $h(t) = 0$), the steady state modal response can be obtained as:

$$\eta_r(t) = \frac{m\omega^2 - i\omega c_a}{\omega_r^2 - \omega^2 + i2\zeta_r\omega_r\omega}\gamma_r^w Y_0 e^{i\omega t} \tag{23}$$

where

$$\gamma_r^w = \int_{x=0}^{L} \phi_r(x)dx = \frac{2\sigma_r}{\lambda_r}\sqrt{\frac{L}{m}} \tag{24}$$

is obtained by integrating Equation (10) over the beam length. Using Equations (8), (10), and (23), one can obtain the expression for the relative response at point x and time t as:

$$w_{rel}(x,t) = 2Y_0 e^{i\omega t}\sum_{r=1}^{\infty}\left[\cosh\frac{\lambda_r}{L}x - \cos\frac{\lambda_r}{L}x - \sigma_r \times\left(\sinh\frac{\lambda_r}{L}x - \sin\frac{\lambda_r}{L}x\right)\right]\frac{\sigma_r\left(\omega^2 - i2\zeta_r^a\omega_r\omega\right)}{\lambda_r\left(\omega_r^2 - \omega^2 + i2\zeta_r\omega_r\omega\right)}. \tag{25}$$

Then, by setting $x = L$ one obtains

$$w_{rel}(L,t) = 2Y_0 e^{i\omega t}\sum_{r=1}^{\infty}\left[\cosh\lambda_r - \cos\lambda_r - \sigma_r(\sinh\lambda_r - \sin\lambda_r)\right]\frac{\sigma_r(\omega^2 - i2\zeta_r^a\omega_r\omega)}{\lambda_r(\omega_r^2 - \omega^2 + i2\zeta_r\omega_r\omega)}. \tag{26}$$

which is the distributed parameter (Euler–Bernoulli model) steady state solution for the relative tip displacement due to harmonic base excitation (when there is no tip mass).

SDOF Model of the Harmonic Base Excitation Problem

Single-degree-of-freedom modeling approach implies describing the dynamics of the point of interest (usually the free end of the beam) in terms of some lumped parameters which are the equivalent mass, stiffness, and the damping of the beam denoted by m_{eq}, k_{eq}, and c_{eq}, respectively (Figure 2(a)). The equivalent stiffness is obtained from the static deflection relation of a cantilevered beam due to a concentrated transverse load at the tip and the equivalent mass is obtained by expressing the total kinetic energy of the beam in terms of the velocity at the tip, for cantilevered end conditions where the base is not moving. However, it should be highlighted at this point that in the base excitation problem (unlike the problem of a beam where the base is not moving) the beam is excited by its own inertia and there is a rigid body inertia contribution to the motion from its distributed mass. In other words, the inertia of the system is not only due to the vibratory motion of the beam but also it is due to the rigid body motion of the beam. This important difference will lead to a correction factor for the SDOF modeling later in this study.

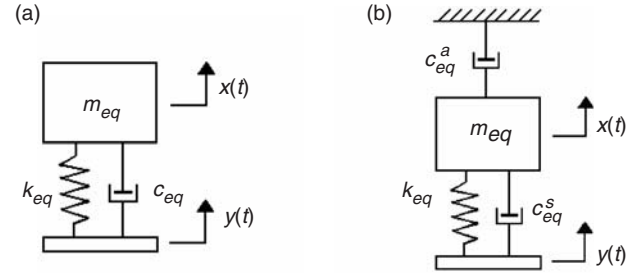

Figure 2. *Lumped parameter models of the base excitation problem: (a) the commonly used representation and (b) the correct representation of air damping.*

The commonly used lumped parameter model is shown in Figure 2(a) and the lumped parameter model with the correct representation of damping is given in Figure 2(b). The correction made is due to the modeling of the external viscous damping (which is indeed the air damping). It is analogous to the Euler–Bernoulli model solution that the structural damping acts on the relative velocity between the mass and the base; however, the air damping acts on the absolute velocity of the mass.

In Figure 2, $y(t)$ is the harmonic base excitation ($y(t) = Y_0 e^{i\omega t}$) whereas $x(t)$ is the absolute response of the mass (i.e., it is the absolute transverse displacement at the free end of the beam). Let the response of the mass relative to the base be $z(t) = x(t) - y(t)$. For the system shown in Figure 2(a), one can obtain the relative motion of the mass as:

$$z(t) = \frac{\omega^2 m_{eq}}{k_{eq} - \omega^2 m_{eq} + i\omega c_{eq}} Y_0 e^{i\omega t} \tag{27}$$

which can be found in any elementary vibration text and which is also frequently referred in order to describe dynamics of vibration energy harvesters.

In Equation (27), $k_{eq} = 3EI/L^3$, $m_{eq} = 33/140\,mL + M_t$ (where M_t is the tip mass, if there is one) and $c_{eq} = 2\zeta\omega_n m_{eq}$ where ζ is the equivalent damping ratio. The (fundamental) natural frequency of the system is simply $\omega_n = \sqrt{k_{eq}/m_{eq}}$. Clearly, this model assumes a single damping coefficient which acts on the relative velocity of the tip mass.

Now, consider the SDOF model presented in Figure 2(b) where air damping and structural damping are treated separately; the former is acting on the absolute velocity of the mass and the latter is acting on the velocity of the mass relative to the base. The air damping coefficient c_{eq}^a is assumed to be proportional to m_{eq} ($c_{eq}^a = a_0 m_{eq}$) whereas the structural damping coefficient c_{eq}^s is assumed to be proportional to k_{eq} ($c_{eq}^s = a_1 k_{eq}$), where a_0 and a_1 are the constants of proportionality. Once again, obtaining the proportionality constants a_0 and a_1 (hence the damping coefficients c_{eq}^a and c_{eq}^s) from experimental measurements requires knowing the damping ratios and natural frequencies of two separate modes of the real (distributed parameter) system (Clough and Penzien, 1975) as in the case of the Euler–Bernoulli model (see Equation (17)). For the SDOF model shown in Figure 2(b), the relative response of the tip mass can be expressed as:

$$z(t) = \frac{\omega^2 m_{eq} - i\omega c_{eq}^a}{k_{eq} - \omega^2 m_{eq} + i\omega c_{eq}} Y_0 e^{i\omega t}. \tag{28}$$

Here, $c_{eq}^a = 2\zeta^a \omega_n m_{eq}$ and $c_{eq} = c_{eq}^a + c_{eq}^s = 2\zeta\omega_n m_{eq}$, where ζ^a is the viscous air damping ratio. Clearly, in the commonly referred Equation (27), the forcing term due to air damping is missing. In their SDOF electromechanically coupled equations, duToit et al. (2005) suggested representing all sources of mechanical damping by a single damping ratio acting on the relative velocity of the tip mass. It is obvious from this discussion that such an approach without any justification is incorrect. However, for the case where the damping ratio ζ^a due to the medium (which is generally air) is very low, it is reasonable to expect the forcing term $-i\omega c_{eq}^a$ coming from the air damping to be much less than the inertial forcing term $\omega^2 m_{eq}$ and consequently Equation (28) reduces to Equation (27). For a nondimensional comparison, dividing both of these forcing terms by m_{eq} gives the inertia contribution as ω^2 and the air damping contribution as $-i2\zeta^a\omega_n\omega$. For the case of excitation at the natural frequency ($\omega = \omega_n$), how the percentage forcing contribution of air damping varies with ζ^a is shown in Figure 3 (which is simply the plot of $2\zeta^a/\sqrt{1+(2\zeta^a)^2} \times 100$). As can be seen from the figure, the excitation amplitude coming from the air damping is <10% of the total excitation (inertial and damping) if $\zeta^a < 0.05$. The conclusion of this short discussion is that the SDOF model of the harmonic base excitation problem given by Figure 2(a) and Equation (27) implicitly assumes the damping excitation of the medium to be sufficiently low when compared to inertial excitation.

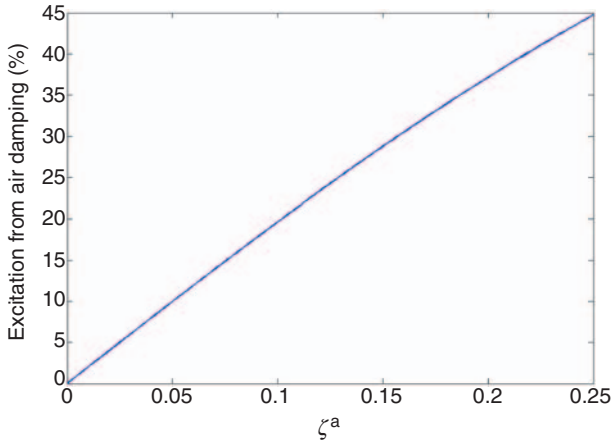

Figure 3. *Contribution to the total excitation from air damping as a function of air damping ratio (for excitation at resonance).*

Comparison of the Euler–Bernoulli and the SDOF Model Predictions

Consider the expressions of the relative tip response obtained by using the Euler–Bernoulli and the SDOF models, which are Equations (26) and (28), respectively. As mentioned previously, for the case of light air (medium) damping (i.e., for $\zeta^a, \zeta_r^a \ll 1$) the excitation due to the inertia term dominates the numerators of Equations (26) and (28) and these equations can be reduced to

$$w_{rel}(L,t) = 2\omega^2 Y_0 e^{i\omega t} \sum_{r=1}^{\infty} \frac{\sigma_r[\cosh\lambda_r - \cos\lambda_r - \sigma_r(\sinh\lambda_r - \sin\lambda_r)]}{\lambda_r\left(\omega_r^2 - \omega^2 + i2\zeta_r\omega_r\omega\right)} \tag{29}$$

$$z(t) = \frac{\omega^2}{\omega_n^2 - \omega^2 + i2\zeta\omega_n\omega} Y_0 e^{i\omega t}, \tag{30}$$

respectively.

The tip motion to base motion ratio gives the relative motion transmissibility function, which forms an appropriate nondimensional basis for comparing the Euler–Bernoulli and the SDOF models. These relative motion transmissibility functions can be extracted from Equations (29) and (30) as:

$$T_{rel}^{EB}(\omega,\zeta_r) = 2\omega^2 \sum_{r=1}^{\infty} \frac{\sigma_r[\cosh\lambda_r - \cos\lambda_r - \sigma_r(\sinh\lambda_r - \sin\lambda_r)]}{\lambda_r\left(\omega_r^2 - \omega^2 + i2\zeta_r\omega_r\omega\right)} \tag{31}$$

$$T_{rel}^{SDOF}(\omega,\zeta) = \frac{\omega^2}{\omega_n^2 - \omega^2 + i2\zeta\omega_n\omega} \tag{32}$$

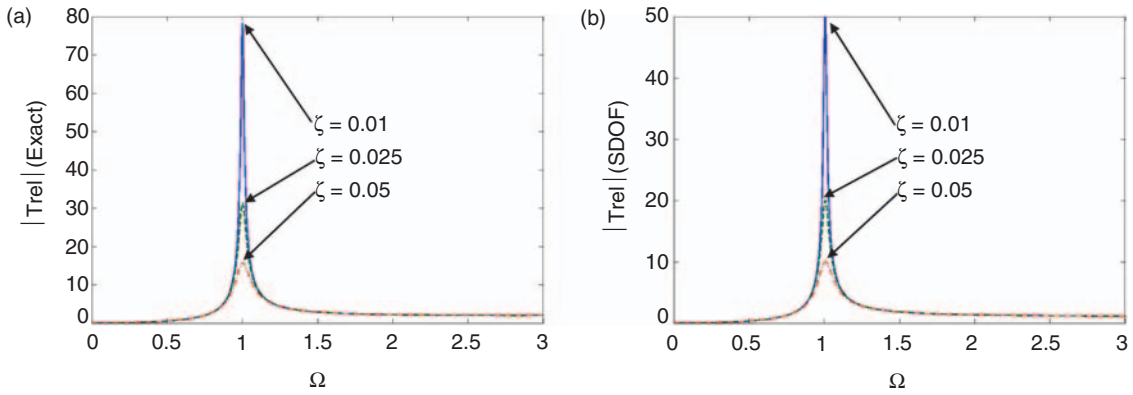

Figure 4. *Relative motion transmissibility functions for transverse vibrations of a cantilevered beam without a tip mass: (a) Euler–Bernoulli model and (b) SDOF model.*

where $T_{\text{rel}}^{\text{EB}}$ and $T_{\text{rel}}^{\text{SDOF}}$ are for the Euler–Bernoulli and the SDOF models, respectively. Note that the Euler–Bernoulli and the SDOF natural frequencies are not identical since the natural frequency prediction of the latter model (which is due to $\omega_n = \sqrt{k_{\text{eq}}/m_{\text{eq}}}$) is slightly different from that of the former model (which is due to Equation (14)). It should be noted from Equations (31) and (32) that these are also functions of the damping ratios. Therefore, it is required to compare the results of these transmissibility functions for different values of damping ratio. Here, three different damping ratio values ($\zeta = 0.01,\ 0.025,\ 0.05$) are used for comparison of the models. The relative motion transmissibility functions given by Equations (31) and (32) are shown in Figure 4(a) and (b), respectively. For convenience, the excitation frequency ω is normalized with respect to the fundamental natural frequency (of the Euler–Bernoulli beam model as it is assumed to be the accurate one) and therefore the frequency axis is denoted by $\Omega = \omega/\omega_1$. As can be seen from Figure 4, the frequency of maximum relative motion transmissibility corresponds to $\Omega \cong 1$ in both models since the SDOF approach gives a good estimate of fundamental natural frequency. However, it is not possible to make the same conclusion for the amplitude-wise results. It is clear from Figure 4 that the peak values for the same damping ratios are different for the Euler–Bernoulli model and the SDOF model predictions.

The relative percentage error in the SDOF solution as a function of dimensionless frequency ratio is given by Figure 5. As can be seen from the figure, the error due to using the SDOF approach for predicting the relative motion at the tip of the beam is very high. In the vicinity of the first natural frequency (i.e., at $\Omega \cong 1$), the error of the SDOF model can be >35% regardless of the damping ratio. The interesting behavior in the error plot at resonance is due to the error in the natural frequency predicted by the SDOF approach (as mentioned previously). If the SDOF natural frequency were taken to be identical to the first natural frequency of the Euler–Bernoulli model, one would obtain a smooth behavior in the error. Figure 5 shows that the important error is in the prediction of the relative motion amplitude rather than the natural frequency. Of course at higher excitation frequencies, the error in SDOF model increases drastically since the higher vibration modes cannot be captured by the SDOF approach.

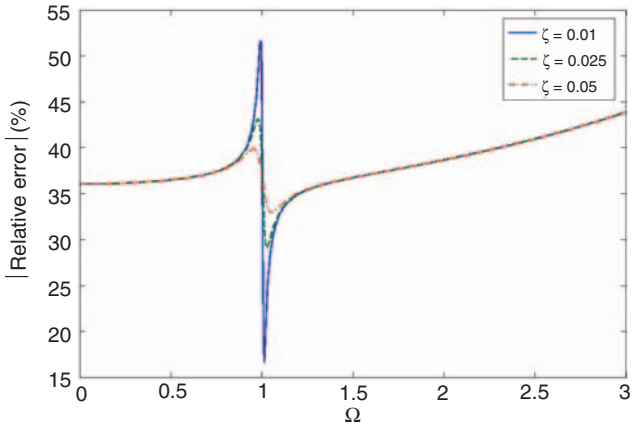

Figure 5. *Error in the relative motion transmissibility due to using the SDOF model for a cantilevered beam without a tip mass in transverse vibrations.*

CORRECTION OF THE SDOF MODEL FOR TRANSVERSE VIBRATIONS

Correction Factor for the SDOF Model

Since much of the harvesting literature uses SDOF modeling for design and optimization, a correction factor is presented for using the simplified SDOF model. Consider the relative motion transmissibility function of the Euler–Bernoulli model given by Equation (31). If the beam is excited around its first natural frequency, taking only the first term in the summation sign (neglecting the terms for $r \geq 2$) gives a good approximation for

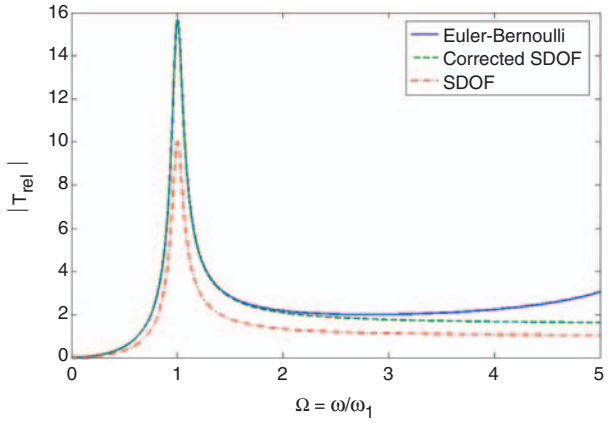

Figure 6. *Relative motion transmissibility functions obtained by the Euler–Bernoulli, corrected SDOF and the original SDOF models for $\zeta = 0.05$.*

the resulting motion transmissibility. This reduced form of the Euler–Bernoulli model solution is denoted by $T_{\text{rel}}^{\text{EB}*}$:

$$T_{\text{rel}}^{\text{EB}*}(\Omega, \zeta) = \frac{\mu_1 \Omega^2}{1 - \Omega^2 + i2\zeta\Omega} \tag{33}$$

where $\Omega = \omega/\omega_1$ is used and μ_1 is defined as the correction factor for the first transverse vibration mode of a cantilevered Euler–Bernoulli beam without a tip mass. Using $\lambda_1 = 1.87510407$ and $\sigma_1 = 0.734095514$ obtained from Equations (11) and (12) gives the correction factor of the first mode as:

$$\mu_1 = \frac{2\sigma_1[(\cosh\lambda_1 - \cos\lambda_1) - \sigma_1(\sinh\lambda_1 - \sin\lambda_1)]}{\lambda_1} \cong 1.566. \tag{34}$$

It should be noted from Equations (32) and (33) that the reduced form of the Euler–Bernoulli solution for the first mode is indeed the correction factor μ_1 multiplied by the SDOF solution (assuming that the SDOF model natural frequency is accurate so that $\Omega = \omega/\omega_1 = \omega/\omega_n$). Therefore, μ_1 corrects the amplitude of the relative motion obtained by the SDOF solution. The comparison of the relative motion transmissibility functions obtained by using the Euler–Bernoulli model, the SDOF model, and the corrected SDOF model are given in Figure 6 for $\zeta = 0.05$. The agreement between the Euler–Bernoulli Equation (31) and corrected SDOF Equation (33) is very good in a wide frequency band around the resonance and the corrected SDOF relative motion transmissibility function starts deviating in the region of the second natural frequency. The original SDOF prediction, Equation (32), underestimates the relative motion transmissibility amplitude considerably with an error of about at least 35% (see Figure 5).

If the beam is to be excited not at the first natural frequency but at one of the higher mode frequencies, one can obtain the correction factor of the mode of interest (rth mode) from the following relation (Erturk and Inman, 2007)

$$\mu_r = \frac{2\sigma_r[(\cosh\lambda_r - \cos\lambda_r) - \sigma_r(\sinh\lambda_r - \sin\lambda_r)]}{\lambda_r} \tag{35}$$

and then use it in the following expression of reduced relative motion transmissibility

$$T_{\text{rel}}^{\text{EB}*}(\Omega_r, \zeta_r) = \frac{\mu_r \Omega_r^2}{1 - \Omega_r^2 + i2\zeta_r\Omega_r} \tag{36}$$

where the dimensionless frequency ratio is now $\Omega_r = \omega/\omega_r$ and ω_r is the undamped natural frequency of the rth mode obtained from Equation (14) and ζ_r is the modal damping ratio of the rth mode. Note that, since the modal parameters λ_r and σ_r do not depend on the aspect ratio of the beam, the correction factor μ_r of the rth mode is unique in the absence of a tip mass. For instance, the correction factor for the fundamental mode is $\mu_1 \cong 1.566$ for any uniform cantilevered Euler–Bernoulli beam without a tip mass in transverse vibrations (so long as the beam aspect ratio justifies the Euler–Bernoulli beam assumptions). However, the presence of a tip mass affects the correction factor which is discussed in the following section.

Effect of a Tip Mass on the Correction Factor

In some cases, it is required to attach a tip (proof) mass to the bender in order to reduce its natural frequencies and improve its flexibility. When a tip mass is attached to the beam shown in Figure 1 rigidly at $x = L$, the formulation of the base excitation problem requires some modifications (Erturk and Inman, 2007). After the addition of a tip mass, not only the eigenvalue problem is changed due to the variation of the natural boundary conditions at the free end of the beam (yielding a different characteristic equation, eigenvalues, and eigenfunctions) but also the excitation of the beam is changed since the inertia of the tip mass also contributes to the excitation of the beam itself. Expectedly, this modification results in variation of the correction factor defined in the previous section. The variation of the correction factor μ_1 of the fundamental transverse vibration mode with tip mass (M_t) to beam mass (mL) ratio is shown in Figure 7. Note that the possible rotary inertia of the tip mass is neglected for simplicity.

It can be seen from Figure 7 that when there is no tip mass ($M_t/mL = 0$), $\mu_1 \cong 1.566$ as previously obtained, and as M_t/mL becomes larger, μ_1 approaches to unity. The important conclusion drawn from Figure 7 is that the uncorrected SDOF model can be used safely only when the tip mass is much larger than the beam mass. The following quadratic polynomial ratio obtained by using the Curve Fitting Toolbox of MATLAB®

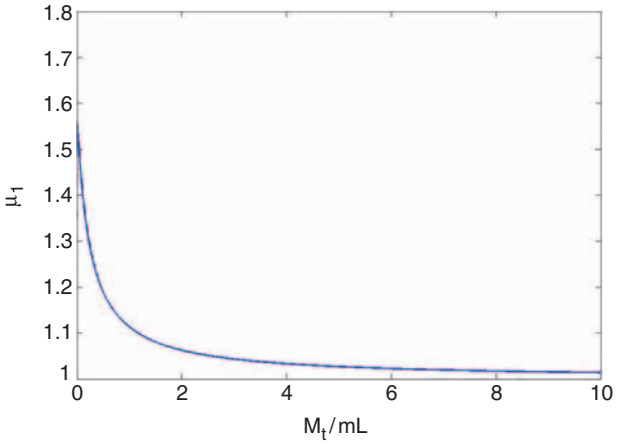

Figure 7. *Variation of the correction factor for the fundamental transverse vibration mode with tip mass to beam mass ratio.*

allows calculating μ_1 with an error $<9\times10^{-3}$ for all values of M_t/mL:

$$\mu_1 = \frac{(M_t/mL)^2+0.603(M_t/mL)+0.08955}{(M_t/mL)^2+0.4637(M_t/mL)+0.05718}. \quad (37)$$

BASE EXCITATION PROBLEM FOR LONGITUDINAL VIBRATIONS

The base excitation problem for a bender in transverse vibrations has been discussed in detail and this section summarizes the same problem for longitudinal vibrations. The bar shown in Figure 8 is subjected to the arbitrary translation of its base which is denoted by $u_b(t)$. For the case of an energy harvester, the main bar is a PZT stack and longitudinal strains associated with the vibratory motion results in electric charge and the electrodes that capture the charge developed are located at the boundaries of the stack being perpendicular to the x-axis.

The equation of motion for the longitudinal free vibrations of a bar can be written as:

$$EA\frac{\partial^2 u(x,t)}{\partial x^2} + c_s A\frac{\partial^3 u(x,t)}{\partial x^2 \partial t} - c_a\frac{\partial u(x,t)}{\partial t} - m\frac{\partial^2 u(x,t)}{\partial t^2} = 0 \quad (38)$$

where EA is the axial stiffness (E is the Young's modulus and A is the cross-sectional area) and m is the mass per unit length of the bar and the absolute motion at any point x can be represented by $u(x,\ t) = u_b(t) + u_{rel}(x,\ t)$. The damping mechanism is again represented by two terms[3]: c_s is due to internal (structural) friction

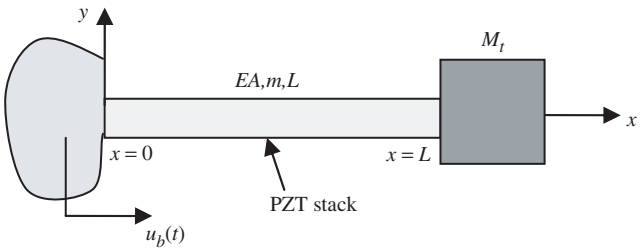

Figure 8. *Cantilevered bar (PZT stack) with a tip mass under arbitrary translational base motion.*

and c_a accounts for external viscous (air) damping. Both of these damping mechanisms are proportional which allows using the corresponding undamped eigenfunctions in the modal analysis.

After following the same steps given for transverse vibrations, the relative response at the free end of the bar can be obtained as:

$$u_{rel}(x,t) = \sum_{r=1}^{\infty}\frac{\varphi_r(x)}{\omega_{rd}}\int_{\tau=0}^{t} N_r(\tau)e^{-\zeta_r\omega_r(t-\tau)}\sin\omega_{rd}(t-\tau)d\tau \quad (39)$$

where the modal forcing function is[4]

$$N_r(t) = \frac{d^2u_b(t)}{dt^2}\left[m\int_{x=0}^{L}\varphi_r(x)dx + M_t\varphi_r(L)\right]. \quad (40)$$

It should be noted from Equation (40) that the excitation coming from the tip mass is directly considered in the modal forcing term.

The undamped natural frequency ω_r of the rth mode is simply

$$\omega_r = \alpha_r\sqrt{\frac{EA}{mL^2}} \quad (41)$$

and ω_{rd} in Equation (39) is the damped natural frequency obtained from $\omega_{rd} = \omega_r\sqrt{1-\zeta_r^2}$ where ζ_r is the modal damping ratio of the rth mode. The mass normalized eigenfunction $\varphi_r(x)$ of the rth mode can be expressed as:

$$\varphi_r(x) = \frac{1}{\sqrt{mL/2(1-\sin 2\alpha_r/2\alpha_r)+M_t\sin^2\alpha_r}}\sin\frac{\alpha_r}{L}x. \quad (42)$$

Here, the eigenvalues (α_r s) are the roots of the characteristic equation

$$\frac{M_t}{mL}\alpha\sin\alpha - \cos\alpha = 0. \quad (43)$$

[3]Although the same notation for the damping coefficients is used in the transverse vibration case, they are not necessarily identical.

[4]Forcing due to air damping is neglected for convenience.

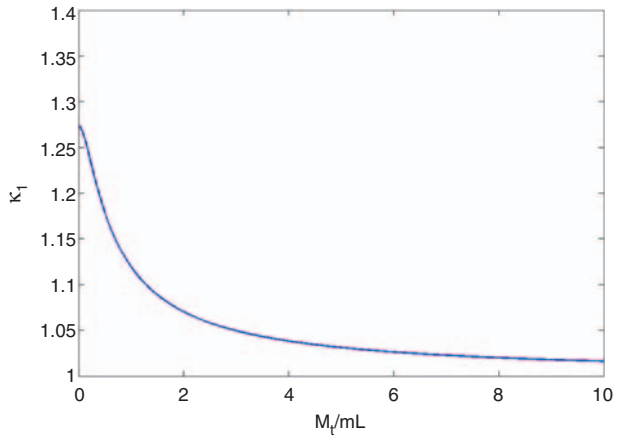

Figure 9. *Variation of the correction factor for the fundamental longitudinal vibration mode with tip mass to bar mass ratio.*

For harmonic base input, $u_b(t) = X_0 e^{i\omega t}$, the steady state relative response at the tip of the bar becomes

$$u_{rel}(L,t) = \sum_{r=1}^{\infty} \times \frac{\sin\alpha_r[(1-\cos\alpha_r)/\alpha_r + M_t/mL\sin\alpha_r]\omega^2 X_0 e^{i\omega t}}{\left[(2\alpha_r - \sin 2\alpha_r)/4\alpha_r + M_t/mL\sin^2\alpha_r\right]\left(\omega_r^2 - \omega^2 + i2\zeta_r\omega_r\omega\right)}. \quad (44)$$

Therefore, the relative motion transmissibility between the tip of the bar and the base can be extracted as:

$$T_{\text{rel}}(\omega,\zeta_r) = \frac{u_{\text{rel}}(L,t)}{X_0 e^{i\omega t}} = \sum_{r=1}^{\infty} \frac{\kappa_r \omega^2}{\omega_r^2 - \omega^2 + i2\zeta_r\omega_r\omega} \quad (45)$$

where

$$\kappa_r = \frac{\sin\alpha_r(1-\cos\alpha_r)/\alpha_r + M_t/mL\sin\alpha_r)}{(2\alpha_r - \sin 2\alpha_r)/4\alpha_r + M_t/mL\sin^2\alpha_r} \quad (46)$$

is the correction factor for the SDOF model of the rth mode for longitudinal vibrations. Note that, κ_r is a function of M_t/mL and α_r due to Equation (46), and α_r is a function of M_t/mL from Equation (43). Therefore, the correction factor κ_r is a function of M_t/mL. In the absence of a tip mass ($M_t/mL = 0$), the correction factor for the fundamental mode can explicitly be obtained from Equations (43) and (46) as $\kappa_1 = 4/\pi \cong 1.273$. However, in the presence of a tip mass, the transcendental equation given by Equation (43) must be solved numerically to obtain the correction factor. The variation of the correction factor of the fundamental mode (κ_1) with M_t/mL is given in Figure 9.

As in the case of transverse vibrations, the correction factor tends to unity as tip mass to bar mass ratio increases, meaning that the uncorrected SDOF model can be used only for the bars whose tip mass is much larger than the bar mass. The following quadratic polynomial ratio obtained by using the Curve Fitting Toolbox of MATLAB® represents the behavior of the correction factor shown in Figure 9 successfully with a maximum error $<4.5 \times 10^{-2}\%$ for all values of M_t/mL:

$$\kappa_1 = \frac{(M_t/mL)^2 + 0.7664(M_t/mL) + 0.2049}{(M_t/mL)^2 + 0.6005(M_t/mL) + 0.161}. \quad (47)$$

CORRECTION FACTOR IN THE ELECTROMECHANICALLY COUPLED SDOF EQUATIONS

So far, the base excitation problem has been discussed both for transverse and longitudinal vibrations. This section briefly discusses the relevance of the correction factor to the electromechanically coupled equations. The procedure of obtaining the electromechanically coupled equations of a piezoelectric vibration energy harvester involves applying d'Alambert's principle (or Newton's second law) for the beam/bar in mechanical domain, Kirchhoff's loop law for the circuit in electrical domain as well as including the electromechanical coupling effects coming from the well-known constitutive relations

$$S = s^E T + dE \quad D = dT + \varepsilon^T E \quad (48)$$

where S is the strain, T is the stress, D is the electric displacement, E is the electric field, d is the piezoelectric constant, S^E is the mechanical compliance at constant electric field, and ε^T is the permittivity at constant stress.

The 'general 1-D model of piezoelectric vibration energy harvester' shown in Figure 10 as well as the sample numerical values shown in the same figure are from a recent work by duToit et al. (2005) and these data are used for the purpose of demonstration here. The electromechanically coupled equations of their model are given as[5]

$$\frac{d^2 u_{\text{rel}}}{dt^2} + 2\zeta_m\omega_n\frac{du_{\text{rel}}}{dt} + \omega_n^2 u_{\text{rel}} - \omega_n^2 d_{33} v = -\frac{d^2 u_b}{dt^2} \quad (49)$$

$$R_{\text{eq}} C_p \frac{dv}{dt} + v + m_{\text{eq}} R_{\text{eq}} d_{33}\omega_n^2 \frac{du_{\text{rel}}}{dt} = 0 \quad (50)$$

where m_{eq} is the equivalent mass of the bar, ζ_m is the mechanical damping ratio, ω_n is the natural frequency, d_{33} is the piezoelectric constant, R_{eq} is the equivalent resistance, C_p is the capacitance, u_b is the harmonic base

[5]The variables have been adapted to the notation in our text.

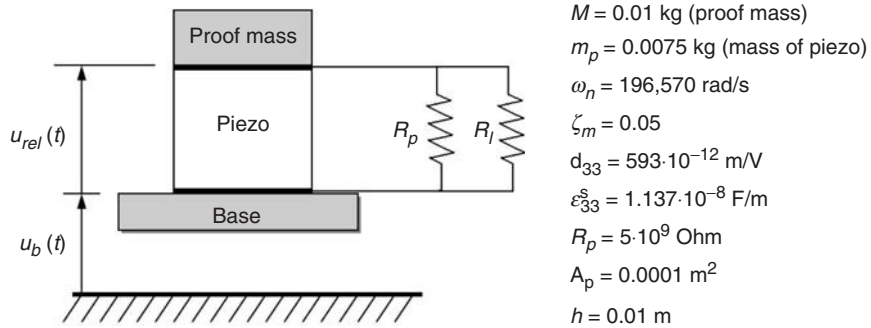

Figure 10. *General 1-D model of piezoelectric vibration energy harvester with sample numerical values used by duToit et al. (2005).*

displacement, u_{rel} is the relative displacement of the proof mass, and v is the voltage output. Discussing the completeness of the electrical loop equation given by Equation (50) is not the aim of this section. However, based on the previous discussion, it is known that the mechanical equilibrium equation given by Equation (49) may need a correction factor. From the numerical values given in Figure 10, the tip mass to bar mass ratio of this sample device is $M_{\text{t}}/mL \cong 1.33$. From Figure 9 or Equation (47), the correction factor for the fundamental mode becomes $\kappa_1 \cong 1.0968$. Therefore, the corrected form of Equation (49) is

$$\frac{d^2u_{\text{rel}}}{dt^2} + 2\zeta_{\text{m}}\omega_{\text{n}}\frac{du_{\text{rel}}}{dt} + \omega_{\text{n}}^2 u_{\text{rel}} - \omega_{\text{n}}^2 d_{33} v = -\kappa_1 \frac{d^2u_{\text{b}}}{dt^2}. \quad (51)$$

It should be mentioned that the resulting relative motion and the voltage amplitudes are proportional to the amplitude of the right-hand side of Equation (51) whereas the power output is proportional to the square of this term[6]. If the correction factor is not used, all of these variables are underestimated. In such a case, the error in the relative tip motion and the voltage amplitudes is about 8.83% whereas the error in the estimated power amplitude is about 16.9%.

VOLTAGE ACROSS THE PZT AND STRAIN NODES OF A CANTILEVERED BENDER

Reconsider the bender shown in Figure 1 which is excited due to the arbitrary translation (in the transverse direction) and small rotation of its base. The aim of this section is to estimate the open-circuit voltage across the PZT at a certain instant of the vibratory motion and to investigate the effects of vibration mode shapes on the electrical outputs of the bender. The approach used by Dosch et al. (1992) for modeling a self-sensing PZT actuator will be followed for obtaining the expression of the voltage output. Note that, the following simple analysis ignores the backward coupling in the mechanical domain. A particular effect of backward coupling is variations in the natural frequencies (short-circuit and open-circuit resonance frequencies) as described by Erturk and Inman (2008). Backward coupling does not alter the results of the below practice since the form of the forcing term in the electrical equation is the same in both cases (with and without backward coupling).

Since no external electric field is applied on the PZT ($E = 0$), the second constitutive relation given by Equations (48) reduces to

$$D_3 = d_{31} T_1 \quad (52)$$

where 1 and 3 directions are coincident with x- and y-axes, respectively. It is clear from Equation (52) that in order to obtain the electric displacement, it is required to find the axial stress which is related to strain from Hooke's law. Note that the axial bending strain $S_1(x, t)$ at a point of interest is a function of the radius of curvature $\rho(x, t)$ of the neutral axis and the distance h_{c} of that point form the neutral axis (Beer and Johnston, 1992):

$$S_1(x, t) = -\frac{h_{\text{c}}}{\rho(x, t)} \quad (53)$$

where the radius of curvature is related to the transverse deflection by

$$\frac{1}{\rho(x, t)} = \frac{\partial^2 w_{\text{rel}}(x, t)}{\partial x^2}. \quad (54)$$

Here, the general form of transverse deflection $w_{\text{rel}}(x, t)$ is as given by Equation (22). Then, using Hooke's law along with Equations (52)–(54) gives the electric displacement as

$$D_3(x, t) = -d_{31} Y_{\text{p}} h_{\text{c}} \frac{\partial^2 w_{\text{rel}}(x, t)}{\partial x^2} \quad (55)$$

where Y_{p} is the Young's modulus of the PZT layer. Note that h_{c} is the distance between the center of the PZT layer (in thickness direction) and the neutral axis of the beam.

[6]The respective expressions of relative tip displacement, voltage and power output for harmonic base input can be found in the work of duToit et al. (2005).

The electric charge $q(t)$ collected by the electrodes can be obtained by integrating the electric displacement over the electrode area as

$$q(t) = \int_A \underset{\sim}{D} \cdot \underset{\sim}{n}\, dA = -\int_{x=0}^{L} d_{31} Y_p h_c b \frac{\partial^2 w_{rel}(x,t)}{\partial x^2} dx \quad (56)$$

where n is the unit outward normal and b is the width of the PZT layer. Using the general form of the relative displacement given by Equation (22) in Equation (56), one can obtain

$$q(t) = -d_{31} Y_p h_c b \sum_{r=1}^{\infty} \int_{x=0}^{L} \frac{d^2\phi_r(x)}{dx^2} dx \frac{1}{\omega_{rd}} \times \int_{\tau=0}^{t} N_r(\tau) e^{-\zeta_r \omega_r (t-\tau)} \sin \omega_{rd}(t-\tau) d\tau. \quad (57)$$

After evaluating the spatial integral (and noting that the relative slope at the root of the bender is zero), the charge on the electrodes can be expressed as:

$$q(t) = -d_{31} Y_p h_c b \sum_{r=1}^{\infty} \left.\frac{d\phi_r(x)}{dx}\right|_{x=L} \times \frac{1}{\omega_{rd}} \int_{\tau=0}^{t} N_r(\tau) e^{-\zeta_r \omega_r (t-\tau)} \sin \omega_{rd}(t-\tau) d\tau. \quad (58)$$

The voltage $v(t)$ across the electrodes can be obtained by dividing the charge on the electrodes to the capacitance C_p of the PZT layer covered by the electrodes:

$$v(t) = -\frac{d_{31} Y_p h_c b}{C_p} \sum_{r=1}^{\infty} \left.\frac{d\phi_r(x)}{dx}\right|_{x=L} \times \frac{1}{\omega_{rd}} \int_{\tau=0}^{t} N_r(\tau) e^{-\zeta_r \omega_r (t-\tau)} \sin \omega_{rd}(t-\tau) d\tau. \quad (59)$$

Note that, while integrating the electric displacement over the electrode area in Equation (56), the electrode area is assumed to be covering the entire beam surface. If the PZT layer and/or the electrodes do not cover the entire bender[7], a more general form of the voltage can be written as:

$$v(t) = -\frac{d_{31} Y_p h_c b}{C_p} \sum_{r=1}^{\infty} \left.\frac{d\phi_r(x)}{dx}\right|_{x=x_1}^{x=x_2} \times \frac{1}{\omega_{rd}} \int_{\tau=0}^{t} N_r(\tau) e^{-\zeta_r \omega_r (t-\tau)} \sin \omega_{rd}(t-\tau) d\tau \quad (60)$$

where $x_1 \le x \le x_2$ is the range covered by the PZT layer and/or the electrodes. If the base of the bender is excited harmonically in the transverse direction (with $g(t) = Y_0 e^{i\omega t}$ and $h(t) = 0$), the steady state voltage can be obtained from

$$v(t) = -\frac{d_{31} Y_p h_c b Y_0 e^{i\omega t}}{C_p} \sum_{r=1}^{\infty} \left.\frac{d\phi_r(x)}{dx}\right|_{x=x_1}^{x=x_2} \frac{(m\omega^2 - i\omega c_a)\gamma_r^w}{\omega_r^2 - \omega^2 + i2\zeta_r \omega_r \omega}. \quad (61)$$

Moreover, if the excitation frequency is the natural frequency of the rth mode ($\omega = \omega_r$), all the terms in the summation sign other than the mode of interest can be ignored, and $v(t)$ becomes

$$v(t) = -\frac{\gamma_r^w d_{31} Y_p h_c b m Y_0 e^{i(\omega_r t - \pi/2)}}{2\zeta_r C_p} \left.\frac{d\phi_r(x)}{dx}\right|_{x=x_1}^{x=x_2} \quad (62)$$

where the forcing due to air damping is neglected. In this type of modal excitation, generally, the mode of interest is the first mode, for which $r = 1$.

The foregoing simple derivation of the voltage output (which ignores the electromechanical coupling effects in mechanical domain) leads to important physical interpretations. The final form of the voltage output that is reduced for the case of excitation at a particular natural frequency, Equation (62), shows that in order to obtain the maximum voltage output one should locate the electrodes such that the difference in the slopes at the electrode boundaries is maximized for that particular mode shape. Moreover, Equation (62) suggests that if the slopes at the boundaries of the electrodes are identical, there is no voltage output.

A more useful discussion is due to Equation (57), where the spatial integration is not performed and the charge developed is proportional to the integral of the curvature of the bender along the portion covered by the electrodes. It should be noted from Equation (57) that the integrand in the charge expression is the curvature of the rth eigenfunction, which is nothing but the measure of axial strain due to bending of the beam (see Equations (53) and (54)). Therefore, the voltage output clearly depends on the area under the strain curve. As a consequence, for the case of excitation at a particular natural frequency (and therefore mode shape), the charge collected by the electrodes and the voltage output depend on the sign alternation in the strain along the electrode length, and reasonably, sign alternation along a single continuous electrode must be avoided. For instance, for the first mode shape (Figure 11(a)), since there is no sign change in the strain (Figure 11(b)), the maximum voltage output can be obtained by covering the entire length of the bender by PZT with continuous electrodes. However, in all higher modes, there exist certain strain nodes where the strain changes sign. Indeed, the number of strain nodes of mode n is simply $n-1$. The normalized mode shapes of the first three modes can be seen in Figure 11(a) and

[7]In such a case, the beam is no longer geometrically uniform, which affects the main formulation (the eigenfunctions, etc.) given in this study. However, if the electrodes are segmented but the PZT layer is continuous, one can still use this formulation to approximate the system dynamics since, in general, the electrodes are very thin when compared to the substructure and the PZT layers.

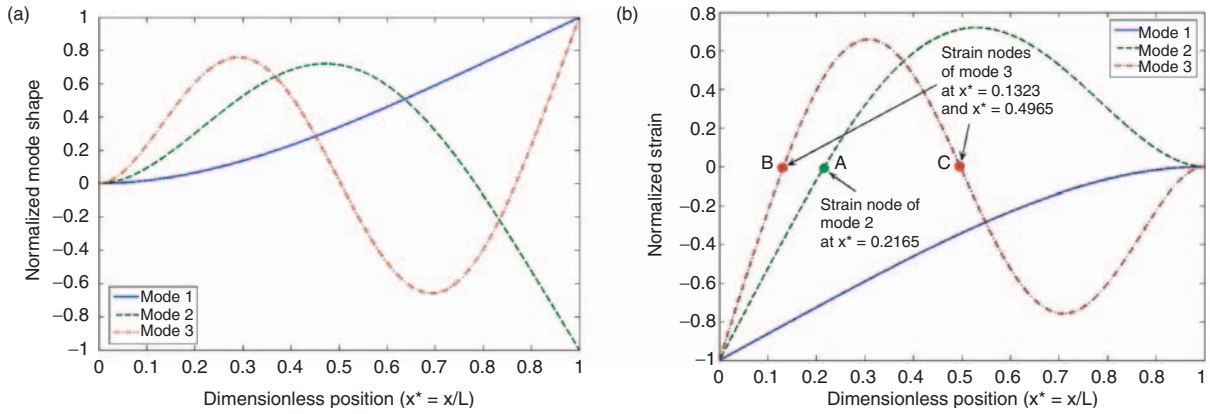

Figure 11. *(a) Normalized mode shapes and (b) strain distributions for the first three modes of a cantilevered beam without a tip mass.*

their respective normalized strain distributions are shown by Figure 11(b) (note that the beam has no tip mass). The second mode has one strain node at $x^* = 0.2165$ (node A) whereas the third mode has two strain nodes at $x^* = 0.1323$ (node B), and $x^* = 0.4965$ (node C) where $x^* = x/L$ is the dimensionless position along the x-axis. If the bender shown in Figure 1 vibrates with the second mode shape (see Figure 11(a)) it can be seen from Figure 11(b) that the left side of node A is in compression when its right side is in tension and vice versa. This is valid for the $n-1$ strain nodes existing in the nth mode shape.

Crawley and de Luis (1987) discussed the importance of strain nodes in their work (which focuses on the converse piezoelectric effect in actuation) with the following words: "...the first mode has no strain nodes. Therefore, if this were the only mode to be excited, the actuators could be placed anywhere along the beam. For maximum effectiveness, they would be placed as near to the root as possible. The second mode has a strain node at $x = 0.216$L. The piezoelectric actuators (PZAs) must be placed away from this point, so that the strain applied over the entire length of the actuator has a constant phase with respect to the homogeneous strain in the beam in this mode. If not, the modal force produced by the actuator will be decreased, since one section of the actuator will be opposing the other ... This reasoning also indicates why it is necessary to use segmented actuators for the control of flexible structures. For the second mode of a cantilevered beam, a PZA located at $x < 0.216$ must be driven 180 deg out of phase with a PZA located at $x > 0.2l6$L". It should be noted that the results of the above formulation in the 'direct sense' are in agreement with the observation of Crawley and de Luis (1987) in the 'converse sense' of using PZT in actuation for structural excitation and control.

Indeed, Cady (1946) discussed this phenomenon about sixty years ago for (longitudinal) vibrations of crystals: "There is no external piezoelectric reaction due to longitudinal deformations when rods with full-length electrodes are excited at an even multiple of the fundamental frequency, since the effects of compressions and extensions in the various segments cancel exactly". He adds in another article of the same book on piezoelectric resonators that "by the use of short (segmented) electrodes, however, intense vibrations, with correspondingly strong electric reactions, can be secured at any value of h (mode number), even or odd ... Resonators with any number of pairs of electrodes can be prepared by silvering or evaporating a uniform metallic deposit on the opposite sides of the bar and then dissolving away metal in the proper regions to produce the desired number of pairs of separate electrodes". Note that his reasoning on even and odd modes is for longitudinal vibrations and the boundary conditions he uses. However, the idea is the same and the 'proper regions' he mentions are just the strain nodes.

In harvesting energy from the vibrations of a bender like the one shown in Figure 1, the location of the electrodes and/or the PZT layer can be very important. For instance, if the PZT layer and the continuous electrodes cover the region between the root of the bender and somewhere around the center of the bender and if the bender vibrates with the second mode shape, one should expect almost no voltage output due to the phase difference between the strains (hence between the electric displacements) at the opposite sides of node A (see Figure 11(b)). In such a case, the charge developed at the opposite sides of the strain node should be collected by separate electrodes so that charge cancellation due to the phase difference in the electric displacements is prevented. Note that the resulting voltages in the electrodes will be 180° out of phase and the circuit that combines these electrodes should be designed accordingly.

If the bender vibrates with a particular mode shape, determining the positions of the strain nodes in order to locate the electrodes accordingly is a

Table 1. Positions of the modal strain nodes for a cantilevered beam without a tip mass in transverse vibrations.

	Dimensionless position on x-axis ($x^* = x/L$)				
Mode 1	–	–	–	–	–
Mode 2	0.2165	–	–	–	–
Mode 3	0.1323	0.4965	–	–	–
Mode 4	0.0944	0.3559	0.6417	–	–
Mode 5	0.0735	0.2768	0.5001	0.7212	–

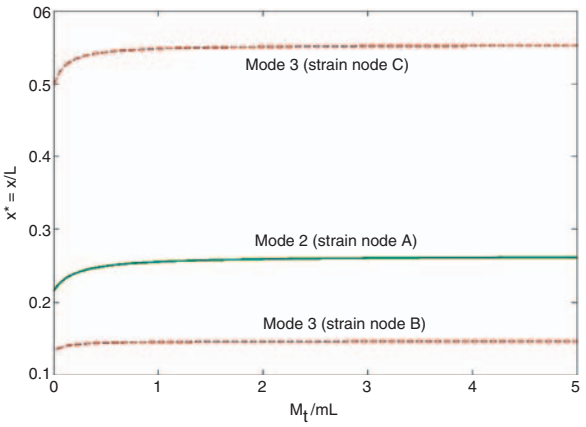

Figure 12. *Variation of the strain node positions for transverse vibrations with tip mass to beam mass ratio (for modes 2 and 3).*

straightforward task. The dimensionless positions of the strain nodes for the first five modes are given by Table 1 for the case where the beam has no tip mass.

The presence of a tip mass results in a variation of strain node positions along the length of the bender. The variations in the positions of the strain nodes (*A*, *B*, and *C* shown in Figure 11(b)) for the second and the third modes are displayed in Figure 12 (rotary inertia of the tip mass is neglected). It should be noted that, in case of transient base excitation or even for the case of harmonic base excitation at non-resonant frequencies, deciding on the location of the electrodes to obtain the maximum voltage output becomes a more involved problem since more than one mode shape with different modal amplitudes contribute to the vibratory motion simultaneously. Yet, in general, only a few modes dominate the vibratory motion which allows ignoring the rest to simplify the problem.

CONCLUSIONS

A cantilevered piezoelectric energy harvester is a typical vibration energy harvester which has been subject to many articles in recent years. In practice, the excitation of these harvesters is generally due to the base motions. In this work, first the general solution of the base excitation problem is reviewed for transverse vibrations of a cantilevered Euler–Bernoulli beam. The base motion is described by arbitrary translation and small rotation and it is not restricted to be harmonic in time. In modeling, damping due to internal friction (strain-rate or the so-called Kelvin–Voigt damping) and the damping due to air (or any other medium) are treated separately. This yields a damping term in addition to the inertial term in the resulting forcing function of the base excitation expression. The former term, however, can be negligible depending on the medium and scale (micro/macro) of the harvester.

The general solution is then reduced for the particular case of harmonic translational base excitation in order to compare the results of the Euler–Bernoulli model with those of the commonly referred SDOF harmonic base excitation model. It is shown that the SDOF model predictions may yield highly inaccurate results. For improving the accuracy of the existing SDOF harmonic base excitation model, a correction factor is introduced. The variation of correction factor with tip (proof) mass to beam mass ratio is given and it is observed that the uncorrected SDOF model can be used only for high tip mass to beam mass ratios. In the absence of tip mass or for the benders with low a tip mass to beam mass ratios, it becomes necessary to use the corrected model.

The discussion made for transverse vibrations is also summarized for the base excitation problem of longitudinal vibrations and some useful equations are presented. Longitudinal vibrations are of interest particularly for harvesters which use PZT stacks. It is shown that the respective SDOF model of the base excitation problem for longitudinal vibrations also requires a correction factor and again the importance of correction factor increases as tip mass to bar mass ratio decreases. The relevance of correction factor to the SDOF electromechanical equations is demonstrated by using an example from the literature.

Finally, simple expressions are derived for the electrical outputs of the PZT in open-circuit conditions and conclusions are drawn regarding the effects of strain nodes of a cantilevered bender based on these equations. Strain nodes (the positions on the bender where strain changes sign) exist for all modes other than the fundamental vibration mode of a cantilevered bender. If the vibration mode of the bender is not the fundamental mode, one should use segmented electrodes for obtaining the maximum voltage output. Otherwise, in case of continuous electrodes, the phase difference in the strains at different sides of a strain node results in charge cancellation in that region, which reduces the charge collected by the continuous electrodes and therefore the voltage output drastically.

ACKNOWLEDGMENTS

The authors gratefully acknowledge the support of the Air Force Office of Scientific Research MURI under grant number F 9550-06-1-0326 'Energy Harvesting and Storage Systems for Future Air Force Vehicles' monitored by Dr B. L. Lee.

REFERENCES

Ajitsaria, J., Choe, S.Y., Shen, D. and Kim, D.J. 2007. "Modeling and Analysis of a Bimorph Piezoelectric Cantilever Beam for Voltage Generation," *Smart Materials and Structures*, 16:447–454.

Banks, H.T. and Inman, D.J. 1991. "On Damping Mechanisms in Beams," *ASME Journal of Applied Mechanics*, 58:716–723.

Beeby, S.P., Tudor, M.J. and White, N.M. 2006. "Energy Harvesting Vibration Sources for Microsystems Applications," *Measurement Science and Technology*, 17:175–195.

Beer, F.P. and Johnston, Jr, E.R. 1992. *Mechanics of Materials*, McGraw-Hill, New York.

Cady, W.G. 1946. *Piezoelectricity*: *An Introduction to the Theory and Applications of Electromechanical Phenomena in Crystals*, McGraw-Hill, New York.

Caughey, T.K. and O'Kelly, M.E.J. 1965. "Classical Normal Modes in Damped Linear Dynamic Systems," *ASME Journal of Applied Mechanics*, 32:583–588.

Clough, R.W. and Penzien, J. 1975. *Dynamics of Structures*, John Wiley and Sons, New York.

Crawley, E.F. and de Luis, J. 1987. "Use of Piezoelectric Actuators as Elements of Intelligent Structures," *AIAA Journal*, 25:1373–385.

Dosch, J.J., Inman, D.J. and Garcia, E. 1992. "A Self-sensing Piezoelectric Actuator for Collocated Control," *Journal of Intelligent Material Systems and Structures*, 3:166–185.

duToit, N.E., Wardle, B.L. and Kim, S. 2005. "Design Considerations for MEMS-Scale Piezoelectric Mechanical Vibration Energy Harvesters," *Journal of Integrated Ferroelectrics*, 71:121–160.

El-Hami, M., Glynne-Jones, P., White, N.M., Hill, M., Beeby, S., James, E., Brown, A.D. and Ross, J.N. 2001. "Design and Fabrication of a New Vibration-based Electromechanical Generator," *Sensors and Actuators A*, 92:335–342.

Erturk, A. and Inman, D.J. 2007. "Mechanical Considerations for Modeling of Vibration-Based Energy Harvesters," *Proceedings of the ASME IDETC* 21*st Biennial Conference on Mechanical Vibration and Noise,* 4–7 September 2007, Las Vegas, NV.

Erturk, A. and Inman, D.J. 2008. "A Distributed Parameter Electromechanical Model for Cantilevered Piezoelectric Energy Harvesters," *ASME Journal of Vibration and Acoustics*, 130.

Fang, H.-B., Liu, J.-Q., Xu, Z.-Y., Dong, L., Chen, D., Cai, B.-C. and Liu, Y. 2006. "A MEMS-Based Piezoelectric Power Generator for Low Frequency Vibration Energy Harvesting," *Chinese Physics Letters*, 23:732–734.

Inman, D.J. 2006. *Vibration with Control*, John Wiley and Sons, Chichester, England.

Jeon, Y.B., Sood, R., Jeong, J.-h. and Kim, S.-G. 2005. "MEMS Power Generator with Transverse Mode Thin Film PZT," *Sensors and Actuators A*, 122:16–22.

Sodano, H., Park, G. and Inman, D.J. 2004. "A Review of Power Harvesting from Vibration Using Piezoelectric Materials," *Shock and Vibration Digest*, 36:197–205.

Stephen, N.G. 2006. "On Energy Harvesting from Ambient Vibration," *Journal of Sound and Vibration*, 293:409–425.

Timoshenko, S., Young, D.H. and Weaver, W. 1974. *Vibration Problems in Engineering*, John Wiley and Sons, New York.

Williams, C.B. and Yates, R.B. 1996. "Analysis of a Micro-Electric Generator for Microsystems," *Sensors and Actuators A*, 52:8–11.